ACS Chemical Neuroscience

Research Article

pubs.acs.org/chemneuro

Binding-Induced Fluorescence of Serotonin Transporter Ligands: A Spectroscopic and Structural Study of 4-(4-(Dimethylamino)phenyl)-1-methylpyridinium (APP$^+$) and APP$^+$ Analogues

James N. Wilson,*[,†] Lucy Kate Ladefoged,[‡] W. Michael Babinchak,[†] and Birgit Schiøtt*[,‡]

[†]Department of Chemistry, University of Miami, Coral Gables, Florida 33124, United States

[‡]inSPIN and iNANO Centers, Department of Chemistry, Aarhus University, 8000 Aarhus C, Denmark

Supporting Information

ABSTRACT: The binding-induced fluorescence of 4-(4-(dimethylamino)-phenyl)-1-methylpyridinium (APP$^+$) and two new serotonin transporter (SERT)-binding fluorescent analogues, 1-butyl-4-[4-(1-dimethylamino)phenyl]-pyridinium bromide (BPP$^+$) and 1-methyl-4-[4-(1-piperidinyl)phenyl]-pyridinium (PPP$^+$), has been investigated. Optical spectroscopy reveals that these probes are highly sensitive to their chemical microenvironment, responding to variations in polarity with changes in transition energies and responding to changes in viscosity or rotational freedom with emission enhancements. Molecular docking calculations reveal that the probes are able to access the nonpolar and conformationally restrictive binding pocket of SERT. As a result, the probes exhibit previously not identified binding-induced turn-on emission that is spectroscopically distinct from dyes that have accumulated intracellularly. Thus, binding and transport dynamics of SERT ligands can be resolved both spatially and spectroscopically.

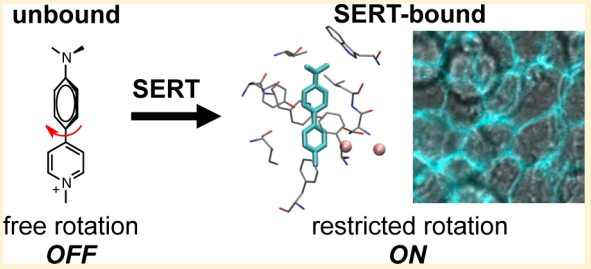

KEYWORDS: *Serotonin, SERT, fluorescence, induced fit docking, quantum polarized ligand docking, LeuT*

Serotonin, or 5-hydroxytryptamine (5-HT), is a chemical messenger with a diverse set of functions in the brain as well as the periphery.[1−3] 5-HT distribution and action is regulated by the serotonin transporter (SERT or 5-HTT), which is responsible for removing extracellular serotonin from serum and synaptic clefts following 5-HT release.[4,5] SERT expression and localization has traditionally been ascertained by immunohistochemical techniques[5−7] or radiolabeled ligands.[3,8] Recently, fluorescent substrates of SERT[9,10] and related monoamine transporters (MATs) have been reported.[11−13] These probes and other fluorescent reporters have proven useful for assessing MAT activity in mixed cell populations,[14] visualizing neurotransmitter release,[13,15,16] and studying binding ratios and uptake kinetics.[11,12]

One important group of fluorescent MAT substrates is the class of the environmentally responsive stilbazolium probes, such as 4-(4-(dimethylamino)-styryl)-*N*-methylpyridinium (ASP$^+$), which exhibit so-called "turn-on" emission. The high sensitivity of ASP$^+$ toward its chemical microenvironment is the result of two features of its molecular architecture (Figure 1). First, the presence of an electron donating dimethyl amino group coupled opposite the electron withdrawing *N*-methylpyridinium ring yields a structure with strong charge transfer character in the excited state. More polar solvents or environments help to stabilize this charge transfer state resulting in a shift to lower emission energies as well as emission quenching. The second feature that contributes to the high sensitivity of ASP$^+$ is the ability of the two aromatic rings to twist from coplanarity, that is, increase the dihedral angle between the aniline and pyridinium rings. Twisting to 90° or a perpendicular geometry effectively turns the emission of ASP$^+$ off. Twisting can be limited in viscous solvents or in geometrically confined environments. The binding of ASP$^+$ to the norepinephrine transporter (NET) places the probe in a solvent excluding and more restrictive environment compared with bulk solution.[17] This enables visualization of binding and displacement reported by DeFelice and co-workers.[11,12] ASP$^+$

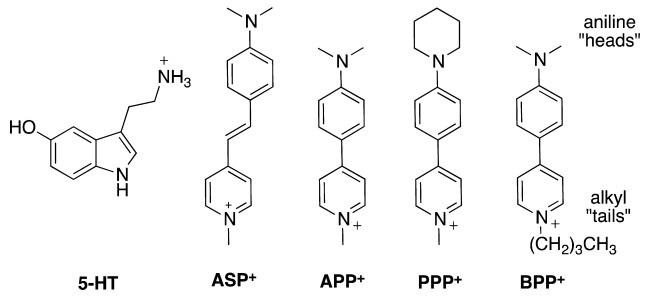

Figure 1. Chemical structures of serotonin (5-HT), ASP$^+$, APP$^+$, and two new fluorescent SERT ligands, PPP$^+$ and BPP$^+$.

Received: December 18, 2013
Accepted: January 24, 2014
Published: January 24, 2014

also exhibits emission upon binding to mitochondria following transport into the cell.

Recently, 4-(4-(dimethylamino)phenyl)-1-methylpyridinium (APP^+, Figure 1) has been reported as a substrate of SERT.[9] APP^+ shares several structural features with ASP^+ and is a highly sensitive turn-on fluorescent probe. However, in contrast to ASP^+, APP^+ was reported to exhibit turn-on fluorescence neither when binding to SERT[9] nor when exposed to cells expressing the dopamine transporter (DAT).[18] Like ASP^+, APP^+ *does* exhibit fluorescence upon binding to mitochondria and nucleoli after transport into the cells.[9,18] This discrepancy in the emission behavior of ASP^+ and APP^+ is intriguing and may reflect alternate binding modes of the two probes, differences in the structural features of the DAT, SERT, and NET binding pockets, or unusual spectroscopic features of the APP^+/SERT complex.

In this contribution, we examine the spectroscopic behavior of APP^+ and two newly synthesized analogues (PPP^+ and BPP^+, Figure 1) in detail. Compounds PPP^+ and BPP^+ were designed to test the limits of APP^+ binding and possess either a bulky anilino "head" in the case of PPP^+ or a longer alkyl "tail" in the case of BPP^+. Both PPP^+ and BPP^+ exhibit solvent-sensitive emission as previously reported for APP^+ and function effectively as turn-on fluorescent probes. We next evaluated our understanding of their photophysical behavior and potential interactions with SERT utilizing the induced fit docking protocol (IFD) entailing full ligand and partial protein flexibility. Both PPP^+ and BPP^+ were found to share similar binding poses and effectively sample the same pocket environment as APP^+. Based on the calculated intramolecular torsions, binding-induced emission was predicted. Confocal microscopy, using a 405 nm diode laser as an excitation source, reveals that APP^+ and the two analogues exhibit turn-on emission when exposed to SERT but not when exposed to DAT or NET. The emission of SERT-bound probes is spectroscopically distinct from the intracellular pool. Thus, while APP^+, PPP^+, and BPP^+ exhibit fluorescence in cells expressing DAT, NET, and SERT, binding to SERT produces a unique spectroscopic signature. This fact, coupled with the relatively high activity of ASP^+ toward DAT and NET,[11] suggests that the combined application of ASP^+ and APP^+ should enable differentiation of catecholaminergic and serotonergic cells in complex tissues.

RESULTS AND DISCUSSION

Photophysical Properties of APP^+ and Analogues. The photophysical properties of APP^+ have been examined in detail by Fromherz and Heilemann.[19] Optical spectroscopy reveals that PPP^+ and BPP^+ exhibit similar photophysical behavior to APP^+, including high sensitivity to their chemical environment due to their ability to access a nonfluorescent, twisted intramolecular charge transfer (TICT) state. By limitation of torsion between the aniline and pyridinium rings, emission is enhanced. Both probes are fluorescent in solvents of higher viscosity, such as octanol (η = 7.24 cP), and quenched in solvents with lower viscosity, such as acetonitrile (η = 0.34 cP), even though they are similar in polarity ($E_T(30)$ = 46.0 and 48.3 kcal/mol for acetonitrile and octanol, respectively).[20] Figure 2 shows the excitation and emission spectra of PPP^+ in octanol (purple lines): PPP^+ has an excitation maximum at 426 nm and an emission maximum at 493 nm; the emission maximum of BPP^+ is slightly red-shifted to 498 nm (see Supporting Information). To eliminate the possibility that

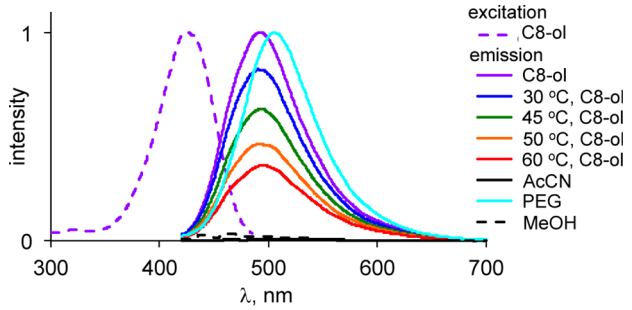

Figure 2. Excitation and emission spectra of PPP^+ in octanol and other solvents show the effect of polarity and visosity, that is, restricted rotation, on emission; APP^+ and BPP^+ exhibit nearly identical spectra, see Supporting Information. Emission is enhanced in more viscous solvents, such as octanol or PEG, compared with polarity matched solvents of lower viscosity, for example, AcCN and MeOH; the temperature dependent emission in octanol also shows the effect of viscosity, eliminating solvent-specific effects. The emission maximum is sensitive to solvent polarity and is red-shifted in PEG relative to octanol.

solvent specific interactions might contribute to the differences in emission intensities, we also examined the effect of temperature-induced changes in viscosity. Increasing the temperature also leads to reduced emission, clearly establishing the relationship between viscosity and fluorescence intensity. Based on these results, we predicted that APP^+, PPP^+, and BPP^+ should exhibit turn-on emission upon binding to SERT, provided that the probes access a pocket that limits access to the quenched TICT state.

APP^+ and analogues PPP^+ and BPP^+ are also sensitive to changes in solvent polarity. For example, the emission maximum of PPP^+ is red-shifted to 505 nm in poly(ethylene glycol) (PEG). Thus, in cases where turn-on emission is observed, the wavelength of the emission maximum can report the average polarity of the chemical microenvironment that the probes experience. Binding-induced emission to SERT may be spectroscopically distinct from emission from mitochondria. Furthermore, if the presence of the bulky head (PPP^+) or tail (BPP^+) forces these probes to adopt different binding poses, this may also be reflected in variations in their emission profiles.

Molecular Docking and Cluster Analysis. We next examined the binding of APP^+, BPP^+, and PPP^+ to a homology model of hSERT[21] based on the bacterial leucine transporter homologue, LeuT (PDB 2A65)[22] to determine the overall geometry, the inter-ring torsions, and the chemical nature of the supporting amino acids and to evaluate whether binding seems possible. The IFD protocol was chosen to accommodate the large ligands in the binding site in an unbiased manor. The resulting poses were clustered according to conformation. A representative low energy conformation of each cluster was further evaluated by quantum polarized ligand docking (QPLD) in order to fully take into account the effect of the charge distribution of the ligands as affected by the protein in order to locate the optimal binding interactions between ligand and hSERT.

The IFD calculation of APP^+ resulted in 95 poses, while the IFD calculations of PPP^+ and BPP^+ gave 13 and 15 poses, respectively. To ensure that the starting conformation of the piperidine ring structure did not affect the results of the IFD, four separate IFD calculations were performed starting from either a chair equatorial, chair axial, twistboat equatorial, or twistboat axial conformation of the piperidine ring.[23] All four

Table 1. Summarized Results of IFD and QPLD Calculations for APP^+, PPP^+, and BPP^+[a]

	IFD			QPLD		
cluster	poses	average Gscore (kcal/mol)	average E-model (kcal/mol)	poses	average Gscore (kcal/mol)	average E-model (kcal/mol)
			APP^+			
A1	9	−7.80 [0.49]	−43.57 [5.15]	3	−3.68 [4.31]	−46.70 [4.84]
A2	67	−7.66 [0.63]	−50.24 [4.73]	2	−6.38 [2.57]	−49.82 [1.77]
A3	2	−6.08 [1.06]	−59.59 [5.36]	1	0.41 [0.00]	−59.67 [0.00]
A4	6	−7.16 [1.21]	−39.88 [8.54]	2	−6.15 [2.47]	−57.37 [0.60]
A5	2	−4.49 [0.17]	−50.00 [6.69]	1	−4.80 [0.00]	−55.07 [0.00]
A6	2	−4.11 [0.34]	−50.60 [2.68]	1	−1.62 [0.00]	−41.94 [0.00]
A7	2	−7.69 [0.15]	−49.59 [0.68]	4	−6.34 [1.79]	−52.81 [1.62]
outliers	5					
			PPP^+			
P1	3	−8.75 [0.42]	−56.37 [4.61	2	−9.05 [0.83]	−66.05 [2.71]
P2	3	−9.00 [0.60]	−53.78 [6.55]	2	−5.52 [0.23]	−63.67 [3.70]
P3	7	−8.48 [1.22]	−56.41 [5.23]	2	−8.86 [0.17]	−67.08 [3.77]
outliers	0					
			BPP^+			
B1	15	−9.40 [0.50]	−61.22 [4.77]	1	−9.78 [0.00]	−63.65 [0.00]
outliers	0					

[a]Standard deviations are in brackets. All data is listed in Table S1 of the Supporting Information.

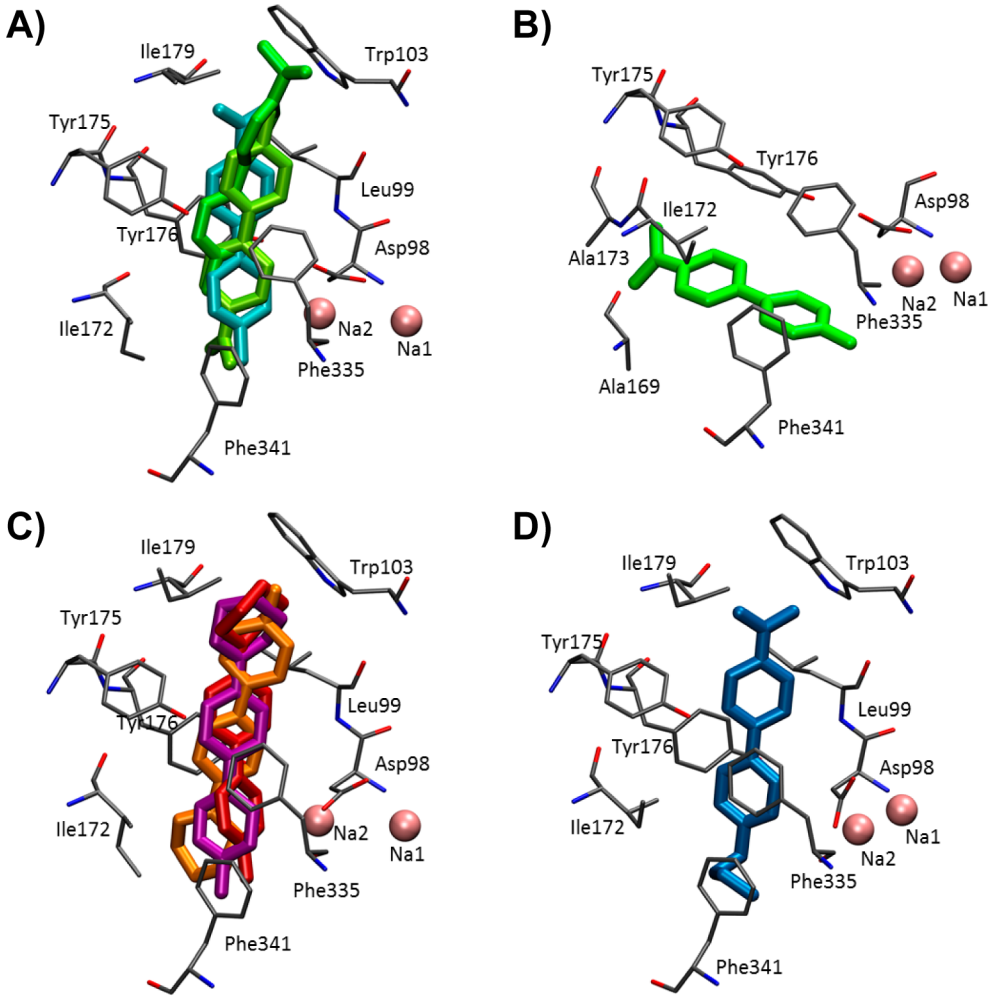

Figure 3. Display of all high-ranked clusters of the IFD into the binding pocket of hSERT, which is colored by atom type. The protein has carbons shown in gray. (A) Display of clusters A1 in bright green, A2 in cyan, and A7 in yellow-green. (B) Display of cluster A4 in lime positioned within the primary binding site. (C) Display of clusters P1 in orange, P2 in red, and P3 in purple. (D) Display of cluster B1 in blue.

dx.doi.org/10.1021/cn400230x | ACS Chem. Neurosci. 2014, 5, 296−304

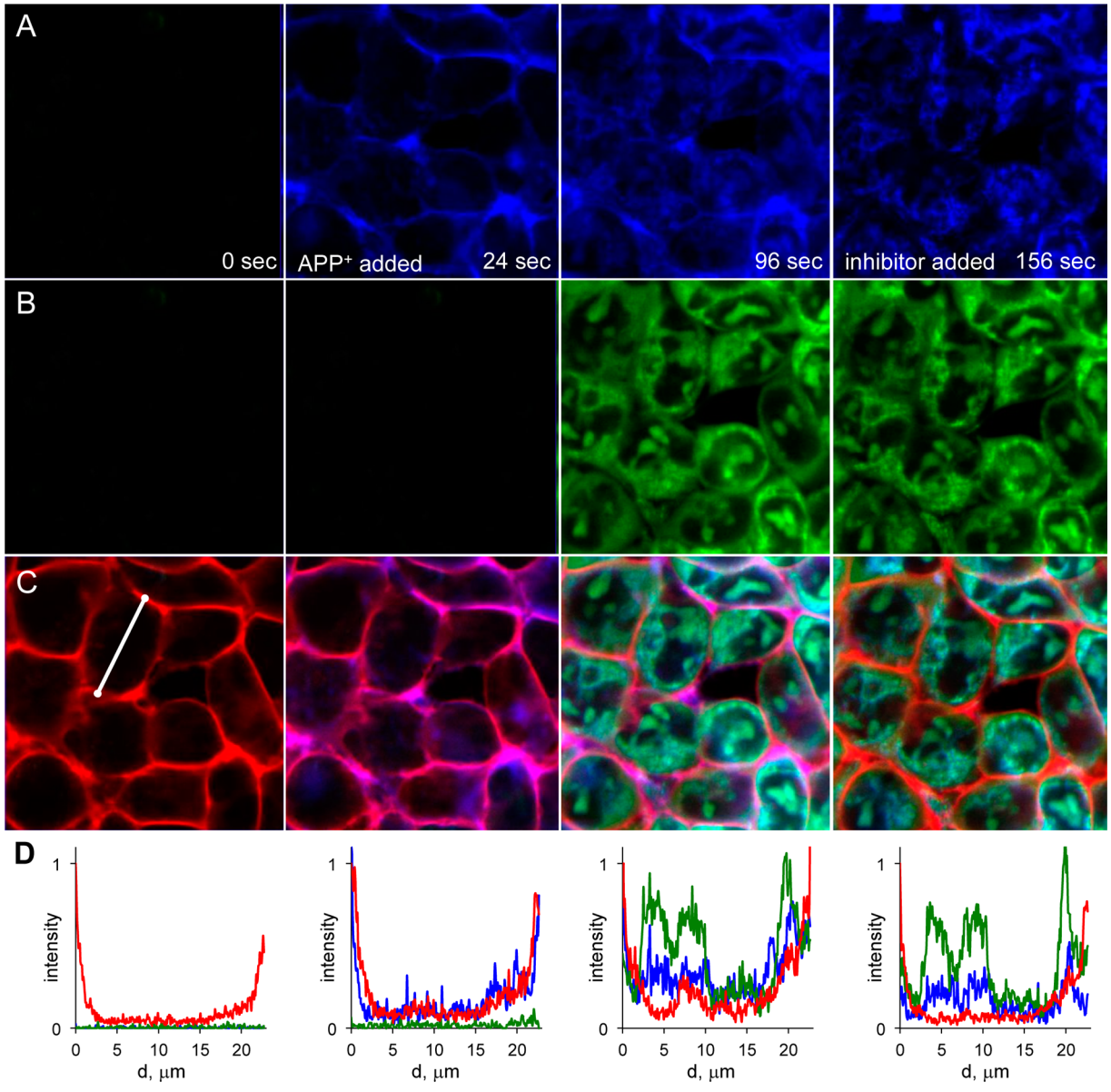

Figure 4. Time course images and analyses of APP^+ binding and transport in hSERT-overexpressing HEK293 cells. Cells were exposed to 2 μM APP^+ after the first image was captured at t = 0 s. A SERT inhibitor, escitalopram, was added at t = 120 s. The white bar in panel C shows the position of the cross sections given in panel D and corresponds to 24 μm. (A) The blue channel, with excitation at 405 nm and emission at 425−500 nm, shows binding to hSERT as well as intracellular accumulation; (B) the green channel, with excitation at 458 nm and emission at 500−600 nm, shows only the intracellular pool with APP^+ localized to mitochondria and nucleoli; (C) the red channel shows the membrane counterstain, CellMask Deep Red, overlaid with blue and green channels. The appearance of emission at t = 24 s in the blue channel colocalizing with the membrane stain (pink areas in C) indicates binding to SERT; this is confirmed by the complete disappearance of the membrane after addition of escitalopram. Uptake of APP^+ (green and blue channels) is slower and the intracellular pool appears after the initial binding to SERT at the membrane (shown at t = 96 s). (D) Cross sections of the blue, green and red channels from a single cell quantitatively show APP^+ binding to and displacement from SERT.

calculations gave very similar results indicating that the starting conformation of the piperidine ring did not bias the IFD calculation (data not shown). Only the results from the lowest energy starting conformation of the piperidine ring (chair axial) will therefore be discussed here. The resulting poses of the IFD calculation of APP^+ were clustered into seven clusters (A1−A7) and five outliers based on the Conformer cluster script of Schrodinger suite 2012 (Table 1). Due to the very poor average XP Gscores of clusters 3, 5, and 6 these were considered unlikely binding modes but were evaluated by QPLD for completeness (see Table 1). The resulting poses of the IFD calculation of PPP^+ and BPP^+ were clustered into three clusters (P1−P3) and a single cluster (B1), respectively. Only APP^+ was able to access the primary binding site of hSERT (A4, Figure 3B), and it was found to be in a manor closely resembling that of previously published data of 1-phenyl-piperazine:[23] The charged nitrogen of APP^+ interacts with the polar Asp98, the backbone of Phe335, or the hydroxyl group of Tyr95, while the remainder of APP^+ primarily interacts with the apolar residues Phe341, Phe335, Ile172, Tyr176, and Ala173 all of which line the binding pocket. The three other clusters of APP^+ (A1, A2, and A7), as well as all clusters of BPP^+ and PPP^+, place the

dx.doi.org/10.1021/cn400230x | ACS Chem. Neurosci. 2014, 5, 296−304

ligands in the extracellular vestibule of hSERT close to the S2 site found in LeuT.[24] APP^+ and PPP^+ were able to bind in either a head-first (A7 and P1) or tail-first fashion (A1, A2, P2, and P3), while BPP^+ was found only to bind in a tail first fashion (B1). Cluster A2 is positioned approximately 3 Å further into the primary binding site than A1, but the two clusters are otherwise highly similar. The clusters of APP^+, PPP^+, and BPP^+ are placed in the S2 site and are very similarly positioned with the apolar portion of the ligand being supported by several aromatic (Phe335, Tyr176, Tyr175, Phe341, and Trp103) and apolar residues (Ile179, Leu99, and Ile172), thus placing the ligands between the aromatic lid of hSERT. The charge of all ligands is supported by interactions with the polar residues Asp98 or Ser438 or the backbone of Phe335 in the case of a tail first entry, but in the case of head-first entry, the charge is left without much support in the vicinity of Glu493. According to the average XP Gscores, all clusters were found to be equally likely to be representative binding modes of APP^+, PPP^+, and BPP^+ in hSERT.

The availability of the TICT state was estimated for APP^+, PPP^+, and BPP^+ when bound to hSERT in either of the two proposed binding sites, the central S1 site or the vestibular S2 site. The torsional angle between the two aromatic units was measured to be less than 50° in 96% of poses and less than 45° in 91% of poses of all ligands indicating that the ligands will not likely access the TICT state while bound to the protein. The modest twist angles also suggest that excitation energies should be relatively high, that is, at shorter wavelengths. While the cationic pyridinium moiety is supported by polar amino acid residues or the amide backbone, the aniline moiety interacts with apolar residues. Thus, redistribution of charge in the excited state is less favorable and the probes should emit at relatively high energies, that is, shorter wavelengths, when bound to hSERT.

A lowest energy representative of each cluster of APP^+, PPP^+, and BPP^+ was further evaluated by QPLD in order to assess the validity of the obtained clusters from the IFD based on more accurate partial charges of the ligands. Clusters A3, A5, and A6 all scored poorly in both the IFD and QPLD calculations and are therefore not considered plausible binding poses and will not be discussed further. The lowest energy pose of the rest of the QPLD output was compared with its input pose, and they were found to be very similar in both conformation and position with a maximum RMSD of 1.13 Å in all clusters except P3 where the lowest energy pose from the QPLD calculations was postioned upside-down relatively to the input IFD pose. The XP Gscores awarded to the best poses of the QPLD were worsened in all clusters except P1, P3, and B1 compared with the XP Gscores given in the IFD, but the Emodel scores were improved in all cases suggesting that there is less conformational strain of the ligands in the poses from QLPD but also indicating that the IFD calculation overestimated the electrostatic reward of poses due to inaccurate partial charges of the ligands. However, the best scoring poses of the QPLD all scored well enough to imply that the clusters are plausible binding modes of APP^+, PPP^+, and BPP^+. The remaining poses of the QPLD were few in number, and most scores of second best poses were poor indicating a rigid binding mode of the ligands in both binding sites.

Confocal Microscopy of APP^+ Binding and Transport. We next evaluated the binding and transport of APP^+ exposed to HEK293 cells expressing hSERT.[25] Based on the optical spectra of the probes and the relatively nonpolar binding site, a 405 nm diode laser was selected as the excitation source because it most closely matches the excitation maximum of the dyes (ca. 425 nm) as shown in Figure 2. Longer wavelength excitation using lines (e.g., 458, 476, 488 nm) of a tunable argon laser is possible because the excitation spectrum extends to approximately 490 nm; however, two issues are present with excitation at these energies: (1) the probes absorb fewer photons, requiring higher laser intensity, and (2) only a fraction of the emission profile will be captured (in either band-pass or long-pass set ups) because the probes emit between 425 and 600 nm.

We imaged the binding, transport, and displacement of APP^+ collecting the emission between 425 and 500 nm in the blue channel (blue) for 405 nm excitation and between 500 and 600 nm in a second channel (green) for 458 nm excitation (Figures 4 and 5). Following addition of APP^+ to hSERT-HEK293 cells, a rapid rise in emission intensity was observed at the cell membrane (blue channel, Figure 4; blue trace, Figure 5)

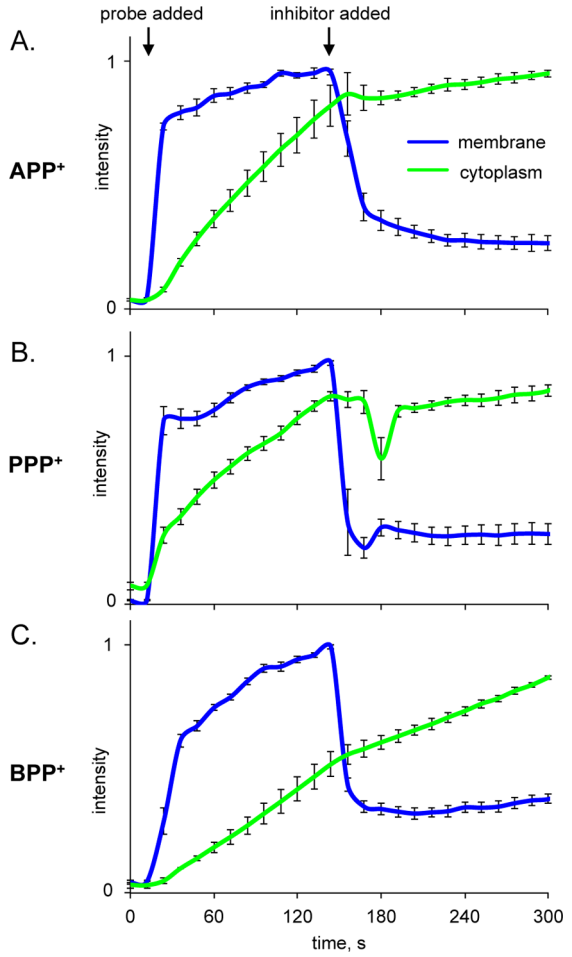

Figure 5. (A) Time-dependent emission profiles of the membrane and cytoplasmic populations of APP^+ reveal that APP^+ rapidly associates with SERT at the membrane (blue trace) and is displaced by escitalopram, an SSRI, or 5-HT, a competitive substrate of SERT. Transport via SERT is constant until addition of a competitive ligand, after which the emission intensity (green trace) plateaus. (B) The binding, displacement and transport kinetics of PPP^+ are identical to those observed for APP^+. (C) BPP^+ shows binding and displacement from SERT but also some nonspecific uptake; intracellular accumulation of BPP^+ is only moderately affected by the addition of escitalopram.

dx.doi.org/10.1021/cn400230x | ACS Chem. Neurosci. 2014, 5, 296−304

colocalizing with a membrane-specific stain, CellMask Deep Red (Life Technologies). As time progressed, emission was also observed within the cells (green channel, Figure 4; green trace, Figure 5), which gradually increased in intensity over time. After 120 s, either 5-HT, the native substrate of SERT, or escitalopram, a selective serotonin reuptake inhibitor (SSRI), was introduced. The addition of either competitive ligand resulted in a rapid decrease in emission intensity at the membrane until the emission intensity within the cell reaches a plateau. The observation of inhibition of APP^+ transport is consistent with the previous report of APP^+ and SERT interactions;[9] however, our observation of membrane-localized emission is unique and appears to be the result of APP^+ binding to SERT rather than a nonspecific interaction with the cell membrane. This notion is supported by the fact that no membrane-localized fluorescence was observed for nontransduced, control HEK293 cells as well as the loss of emission following addition of a competitive substrate (5-HT) or inhibitor (escitalopram). Furthermore, the binding induced emission enhancement appears to be SERT-specific because it is not observed for HEK293 cells overexpressing hDAT or hNET.

Binding and Transport of PPP^+ and BPP^+. All three probes, APP^+, PPP^+ and BPP^+, share similar binding and displacement dynamics; however the intracellular accumulation of BPP^+ and PPP^+ differs from that observed for APP^+ (Figure 4). Upon addition of PPP^+ or BPP^+ to hSERT-HEK293 cells, turn-on emission is observed at the membrane while introduction of either 5-HT or escitalopram reduces the membrane emission. Intracellular accumulation of PPP^+ differs slightly from that observed for APP^+. Following introduction of the probe, emission is observed to increase at the mitochondria, but not nucleoli; the rate of transport is significantly attenuated following addition of a competitive SERT ligand. For BPP^+, different transport dynamics were observed. Addition of 5-HT or citalopram does not lead to a marked decrease in the rate of transport suggesting that transport via SERT is not the primary mode of intracellular accumulation for BPP^+. Instead, it appears that the lipophilic butyl tail renders BPP^+ membrane permeable, which has previously been observed for other cationic and lipophilic dyes such as the membrane stain FM1-43 as well as ASP^+ derivatives possessing alkyl tails.[17] The differences observed in PPP^+ and BPP^+ transport dynamics may be linked to the IFD predicted poses. While APP^+ and PPP^+ were able to bind in both head-first and tail-first poses, BPP^+ was found to only bind tail-first.

Spectroscopic Resolution of SERT-Bound and Intracellular APP^+. Intracellular APP^+ localizes to mitochondria and nucleoli where the probes also are emissive.[9,18] IFD studies (see above) placed APP^+ in a primarily hydrophobic binding pocket supported by aromatic residues. Thus, APP^+ should experience a distinct chemical environment when bound to SERT compared with the interactions with nucleic acids or subcompartments of mitochondria. Because the optical properties of APP^+ are highly dependent on polarity of its microenvironment,[19] we expected that emission from these different populations would vary accordingly. Figure 6 depicts the emission spectra of APP^+ at the membrane, mitochondria, and nucleoli. The emission maximum of SERT-bound APP^+ differs by approximately 40 nm from that observed from the mitochondria- or nucleoli-bound APP^+. The emission is at shorter wavelengths, that is, higher energies, which likely reflects the presence of mainly nonpolar aromatic moieties in the binding pocket. Interestingly, the nucleoli pool of APP^+ can be selectively excited using the 458 nm laser line as evident in Figure 6. APP^+ molecules in the nucleoli appear very faint compared with either the mitochondrial or membrane population when excited at 405 nm (blue channel), while they are clearly evident when excited at 458 (green channel). Conversely, the SERT-bound population of APP^+ does not appear in the green channel with 458 nm excitation and is only visible with 405 nm excitation. This can be attributed to the moderate twist between the anilino and pyridinium rings that is predicted by IFD calculations: increasing the angle between the two π systems will lead to an increased electronic bandgap and require higher excitation energies. The distinct photophysical behavior of SERT-bound and intracellular (i.e., transported) APP^+ may enable these two populations to be differentiated spectroscopically in high throughput fluorescence assays without the need for microscopy-based assays and image analysis.

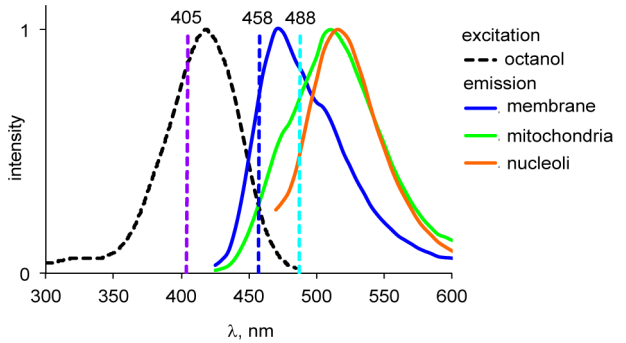

Figure 6. Comparison of optical spectra and available excitation sources for APP^+; the emission spectra were obtained on intact cells using a confocal microscope in $xy\lambda$ mode. The excitation maximum of APP^+ in octanol most closely matches the 405 nm laser line, while 458 nm is also an option. The emission from cellular substructures show distinct spectral profiles; membrane-localized (i.e., SERT-bound) APP^+ exhibits the shortest wavelength emission maximum.

CONCLUSION

Binding induced turn-on emission is an attractive feature of fluorescent probes and ligands because this behavior minimizes background emission from unbound probes and eliminates the need for rinsing steps when imaging. We have demonstrated that APP^+ and analogues BPP^+ and PPP^+ exhibit turn-on emission when binding to SERT. IFD studies reveal that SERT presents a geometrically restrictive ligand binding pocket in which these probes bind amidst mainly aromatic and nonpolar residues. This environment influences the optical properties of the dyes allowing for selective excitation at shorter wavelengths. We have also demonstrated that emission of the SERT bound population is distinct from probes bound to other cellular components, enabling spectroscopic deconvolution of binding and transport without the need for spatial resolution. Based on these results, APP^+ perfectly compliments the binding, transport, and spectroscopic behavior of ASP^+. Employed in tandem, these two probes should enable differentiation of serotonergic and adrenergic cells in tissue presenting both cell types with applications in pharmacological profiling of selective, dual, and triple reuptake inhibitors also possible.

dx.doi.org/10.1021/cn400230x | ACS Chem. Neurosci. 2014, 5, 296−304

METHODS

Experimental Methods. APP^+ was synthesized as previously described[18] and characterized by ^1H NMR, ^{13}C NMR, and HRMS spectroscopies.

Synthesis of 1-Butyl-4-[4-(1-dimethylamino)phenyl]-pyridinium Bromide (BPP^+). 4-[4-(1-Dimethylamino)phenyl]-pyridine[27] (100 mg) was combined with 200 μL of 1-bromobutane and 8.0 mL of toluene in a 20 mL scintillation vial. The reaction mixture was heated at 80 °C for 24 h as a yellow precipitate formed. After the reaction mixture cooled, the crude product was isolated by suction filtration and rinsed with EtOAc. The crude product was crystallized from MeOH/EtOAc to yield 67 mg (52%) of a yellow powder. ^1H NMR (500 MHz, DMSO-d_6): δ (ppm) 0.92 (3H, t, J = 7.5 Hz), 1.31 (2H, quin, J = 7.5 Hz), 1.87 (2H, quin, J = 7.5 Hz), 3.07 (s, 6H), 4.48 (2H, t, J = 7.5 Hz), 6.86 (2H, d, J = 5.0 Hz), 8.03 (2H, d, J = 5.0 Hz), 8.33 (2H, d, J = 7.2 Hz), 8.85 (2H, d, J = 7.2 Hz). ^{13}C NMR (500 MHz, DMSO-d_6): δ (ppm) 13.8, 19.3, 40.1, 59.0, 112.6, 119.2, 121.4, 130.0, 144.1, 153.5, 154.2. IR ν_{max} (cm^{-1}): 715.7, 766.38, 811.9, 837.2, 941.5, 990.0, 1043.0, 1066.6, 1116.0, 1168.0, 1233.6, 1310.9, 1440.0, 1474.2, 1504.9, 1557.9, 1590.0, 2919.8, 2958.4, 3428.2. HRMS (ESI^+) $C_{17}H_{23}N_2$ [M^+]: calculated 255.1859, found. 255.1869. Mp: 249–251 °C.

Synthesis of 1-Methyl-4-[4-(1-piperidinyl)phenyl]-pyridinium Iodide (PPP^+). 4-(4-Fluorophenyl)-1-methylpyridinium iodide[26] (100 mg) was combined with 0.5 mL of piperidine, 100 mg of K_2CO_3, and 2 mL of DMSO in a 20 mL scintillation vial. The reaction mixture was heated at 50 °C for 12 h, developing into a bright yellow solution. After cooling, the solution was filtered, and the solvent was removed under vacuum. The crude product was taken up in the minimum volume of MeOH (~1 mL) and precipitated in EtOAc. Twenty-three mg (17% yield) of a yellow powder was collected by suction filtration (care must be taken because the product is hydroscopic) and dried under vacuum. ^1H NMR (500 MHz, DMSO-d_6): δ (ppm) 1.60 (6H, bs), 3.43 (bs, 4H), 4.22 (3H, s), 7.07 (2H, d, J = 8.3 Hz), 7.99 (2H, d, J = 8.3 Hz), 8.32 (2H, d, J = 5.6 Hz), 8.75 (2H, d, J = 5.6 Hz). ^{13}C NMR (500 MHz, DMSO-d_6): δ (ppm) 24.4, 25.4, 46.7, 48.2, 114.6, 120.5, 121.5, 130.1, 14.0, 153.8(0), 153.8(3). IR ν_{max} (cm^{-1}): 667.0, 745.2, 798.0, 848.4, 918.4, 988.9, 1020.3, 1044.9, 1122.7, 1186.4, 122.4, 1246.0, 1340.6, 1386.3, 1444.8, 1470.9, 1497.3, 1584.3, 1642.0, 2849.6, 2928.0, 3010.8, 3445.1. HRMS (ESI^+) $C_{17}H_{21}N_2$ [M^+]: calculated 255.1699, found 253.1716.

Optical Spectroscopy. Spectroscopy and HPLC grade solvents were utilized for spectroscopic measurements; all path lengths were 1 cm. Emission and excitation spectra were obtained on a PerkinElmer LS55 fluorometer with probe concentrations of 1 μM.

Computational Methods. *Protein Preparation.* The homology model of hSERT used in this study was based on an alignment[28] of the bacterial leucine transporter homologue[22,29] (LeuT) with further optimizations to the extracellular loop 2 of hSERT as described previously.[21,30] This model includes two sodium ions and one chloride ion close to the binding site and has been optimized to accommodate 5-HT.[21]

Ligand Preparation. Ligands APP^+, PPP^+, and BPP^+ were built in Maestro 9.3[31] and were subjected to a conformational search using the OPLS-2005 force field[32] and implicit water in MacroModel 9.9.[33] A minimization step was performed after each iteration of the conformational search using a conjugate gradient algorithm in 5000 steps or until convergence.

Induced Fit Docking. The lowest energy conformation of each ligand was docked using the IFD protocol. This method allows for complete flexibility of the ligand and flexibility of the protein near the binding site, allowing for docking of all ligands into a highly movable protein. First the ligand is docked into the protein using a softened van der Waals (vdW) potential using Glide. This is followed by an optimization of the side chains of the protein near the binding site by Prime, and finally the ligand is redocked using a full vdW potential into the optimized protein using Glide.[34] This protocol employs Glide version 5.8 and Prime version 3.1 from the Schrodinger suite.[35−37] The binding site was defined by residues Gly442, Asp98, Leu431, Thr439, and Ile172.[29,38] The initial docking was performed using the SP scoring function, and the redocking was performed using Glide XP.[39] Up to 100 poses were saved within an energy window of 50 kcal/mol of the lowest scoring pose. All other settings were default settings. Two scoring functions were used to distinguish poses in this study, the Gscore and the E-model score. The Gscore is an empirically determined score that considers the interaction energy between ligand and protein as well as the entropic contribution thus approximating the ligand binding affinity.[37] The E-model score is similar to the Gscore but also takes into account ligand strain and handles the nonbonded interactions more explicitly.

Quantum Polarized Ligand Docking. The lowest energy pose of each cluster from the IFD for each ligand was further evaluated by QPLD in order to fully assess the correct binding mode of each ligand. QPLD is a QM/MM approach that reassigns new partial charges to a ligand using Jaguar based on its position in the binding site thereby acknowledging the polarization experienced by the ligand from the protein, where after the ligand is redocked into the binding site using Glide.[40] Glide version 5.8 and Jaguar version 7.9 was employed by the Schrodinger suite.[35,41] The selected poses from the IFD were used as input directly into the QPLD workflow whereafter the partial charges were recalculated using the 6-31G*/LACVP* basis set and the B3LYP density functional. The redocking was performed with Glide XP, and a maximum of 20 poses were retained. The rest of the settings applied were default settings.

Clustering and Analysis of Poses. The poses from the IFDs were clustered using the Conformer Cluster script available through the Schrodinger Web site. This script was the latest update to the Schrodinger 2012 program suite. The script divides poses into clusters based on the hierarchical clustering algorithm used in Canvas,[42] and the average linking method was chosen to determine the dissimilarity between clusters.

Cell Culture. Parental and HEK293 cells stably expressing SERT (hSERT-HEK293)[25] were cultured as previously described in sterile T-75 flasks.[17] Cells were maintained in DMEM (Dulbecco's modification of Eagle's medium with 4.5 g/L glucose, without L-glutamine and sodium pyruvate) containing 10% dialyzed FBS, 2 mM glutamine, 100 units/mL penicillin, 100 μg/mL streptomycin, and 250 μg/mL Geneticin (hSERT-HEK293 cells only) at 37 °C and 5% CO_2. For imaging experiments, cells were seeded at a density of 10^5 cells/cm^2 in 96-well microtiter plates and incubated for at least 48 h until a visible monolayer was established. Prior to imaging, DMEM was removed from the cells and Leibovitz's L-15 modified (pH 7.3) media with 5% FBS was added to each well. Working solutions were prepared in L-15 media from 1 mM DMSO stocks to concentrations of 100 μM for the fluorescent probes and 10 μM for escitalopram.

Confocal Microscopy. Imaging was performed on a Leica SP5 confocal microscope housed within the UM Biology Imaging Core Facility. All imaging experiments were performed at room temperature (22–25 °C) under normal atmosphere. Excitation was achieved using the 405 nm diode laser or the 458 and 488 nm lines of an argon laser for APP^+ and derivatives as noted in the text; the membrane stain, CellMask Deep Red (CMDR, Life Technologies), was excited at 633 nm. Emission was captured on separate PMTs at wavelengths noted in the text; CMDR emission was captured between 645 and 700 nm. For time course experiments (in *xyt* mode), cells were placed on the imaging stage and brought into focus using phase contrast or the emission of CMDR. Solutions of fluorescent probes or inhibitors were added and gently mixed with pipetting action to produce final concentrations of 2 μM for probes and 2 μM for inhibitors. Images were collected between 2 and 15 s as noted in the text for up to 10 min. For *xyλ* scans, images of whole cells were captured at 5 nm increments with 10 nm band-pass. Images were analyzed using Fiji/ImageJ software (NIH, USA). For time course images, three independent experiments were performed and three or four cells in a field of view were analyzed; error bars show SE.

■ ASSOCIATED CONTENT

Supporting Information

^{1}H and ^{13}C NMR spectra of BPP^+ and PPP^+, summary of IFD and QPLD results, images of BPP^+ and PPP^+ binding to hSERT-HEK293 cells, and control images of APP^+, BPP^+, and PPP^+ with parental HEK293 cells. This material is available free of charge via the Internet at http://pubs.acs.org.

■ AUTHOR INFORMATION

Corresponding Authors

*Email: jnwilson@miami.edu.
*E-mail: birgit@chem.au.dk.

Author Contributions

J.N.W. and B.S. planned the project. W.M.B. and J.N.W. synthesized the fluorescent probes and carried out the optical spectroscopy and imaging experiments. L.K.L performed the docking experiments, and B.S. and L.K.L analyzed the results. The manuscript was written through contributions of all authors.

Funding

This work was supported by the Bankhead-Coley Biomedical Research Program, Grant 3BN08 (J.N.W.), the Danish National Research Foundation, Grant DNRF59, and the Lundbeck Foundation (B.S.).

Notes

The authors declare no competing financial interest.

■ ACKNOWLEDGMENTS

HEK293 cells expressing SERT were a generous gift from Dr. Randy Blakely, Vanderbilt University.

■ ABBREVIATIONS

5-HT 5-hydroxytryptamine; APP^+ 4-(4-(dimethylamino)-phenyl)-1-methylpyridinium; ASP^+ 4-(4-(dimethylamino)-styryl)-*N*-methylpyridinium; BPP^+ 1-butyl-4-[4-(1-dimethylamino)-phenyl]-pyridinium bromide; CT charge transfer; DAT dopamine transporter; IFD induced fit docking; LeuT leucine transporter; NET norepinephrine transporter; QPLD quantum polarized ligand docking; PPP^+ 1-methyl-4-[4-(1-piperidinyl)-phenyl]-pyridinium; SERT serotonin transporter; SSRI selective serotonin reuptake inhibitor; TICT twisted intramolecular charge transfer; vdW van der Waals

■ REFERENCES

(1) Baganz, N. L., and Blakely, R. D. (2013) A dialogue between the immune system and brain, spoken in the language of serotonin. *ACS Chem. Neurosci. 4*, 48−63.

(2) Amireault, P., Sibon, D., and Cote, F. (2013) Life without peripheral serotonin: Insights from tryptophan hydroxylase 1 knockout mice reveal the existence of paracrine/autocrine serotonergic networks. *ACS Chem. Neurosci. 4*, 64−71.

(3) Arango, V., Underwood, M. D., Boldrini, M., Tamir, H., Kassir, S. A., Hsiung, S., Chen, J. J., and Mann, J. J. (2001) Serotonin 1A receptors, serotonin transporter binding and serotonin transporter mRNA expression in the brainstem of depressed suicide victims. *Neuropsychopharmacology 25*, 892−903.

(4) Andersen, J., Stuhr-Hansen, N., Zachariassen, L., Toubro, S., Hansen, S. M., Eildal, J. N., Bond, A. D., Bøgesø, K. P., Bang-Andersen, B., Kristensen, A. S., and Strømgaard, K. (2011) Molecular determinants for selective recognition of antidepressants in the human serotonin and norepinephrine transporters. *Proc. Natl. Acad. Sci. U. S. A. 108*, 12137−12142.

(5) Blakely, R. D., De Felice, L. J., and Hartzell, H. C. (1994) Molecular physiology of norepinephrine and serotonin transporters. *J. Exp. Biol. 196*, 263−281.

(6) McLane, M. W., McCann, U., and Ricaurte, G. (2011) Identifying the serotonin transporter signal in Western blot studies of the neurotoxic potential of MDMA and related drugs. *Synapse 65*, 1368−1372.

(7) Giang, T., Ritze, Y., Rauchfuss, S., Ogueta, M., and Scholz, H. (2011) The serotonin transporter expression in *Drosophila melanogaster*. *J. Neurogenet. 25*, 17−26.

(8) Schenk, S., Hely, L., Lake, B., Daniela, E., Gittings, D., and Mash, D. C. (2007) MDMA self-administration in rats: Acquisition, progressive ratio responding and serotonin transporter binding. *Eur. J. Neurosci. 26*, 3229−3236.

(9) Solis, E., Zdravkovic, I., Tomlinson, I. D., Noskov, S. Y., Rosenthal, S. J., and De Felice, L. J. (2012) 4-(4-(Dimethylamino)-phenyl)-1-methylpyridinium (APP+) is a fluorescent substrate for the human serotonin transporter. *J. Biol. Chem. 287*, 8852−8863.

(10) Oz, M., Libby, T., Kivell, B., Jaligam, V., Ramamoorthy, S., and Shippenberg, T. S. (2010) Real-time, spatially resolved analysis of serotonin transporter activity and regulation using the fluorescent substrate, ASP+. *J. Neurochem. 114*, 1019−1029.

(11) Schwartz, J. W., Blakely, R. D., and DeFelice, L. J. (2003) Binding and transport in norepinephrine transporters. Real-time, spatially resolved analysis in single cells using a fluorescent substrate. *J. Biol. Chem. 278*, 9768−9777.

(12) Schwartz, J. W., Novarino, G., Piston, D. W., and DeFelice, L. J. (2005) Substrate binding stoichiometry and kinetics of the norepinephrine transporter. *J. Biol. Chem. 280*, 19177−19184.

(13) Gubernator, N. G., Zhang, H., Staal, R. G., Mosharov, E. V., Pereira, D. B., Yue, M., Balsanek, V., Vadola, P. A., Mukherjee, B., Edwards, R. H., Sulzer, D., and Sames, D. (2009) Fluorescent false neurotransmitters visualize dopamine release from individual presynaptic terminals. *Science 324*, 1441−1444.

(14) Beikmann, B. S., Tomlinson, I. D., Rosenthal, S. J., and Andrews, A. M. (2013) Serotonin uptake is largely mediated by platelets versus lymphocytes in peripheral blood cells. *ACS Chem. Neurosci. 4*, 161.

(15) Hettie, K. S., Liu, X., Gillis, K. D., and Glass, T. E. (2013) Selective catecholamine recognition with NeuroSensor 521: A fluorescent sensor for the visualization of norepinephrine in fixed and live cells. *ACS Chem. Neurosci. 4*, 918−923.

(16) Klockow, J. L., Hettie, K. S., and Glass, T. E. (2013) ExoSensor 517: A dual-analyte fluorescent chemosensor for visualizing neurotransmitter exocytosis. *ACS Chem. Neurosci. 4*, 1334−1338.

(17) Wilson, J. N., Brown, A. S., Babinchak, W. M., Ridge, C. D., and Walls, J. D. (2012) Fluorescent stilbazolium dyes as probes of the norepinephrine transporter: Structural insights into substrate binding. *Org. Biomol. Chem. 10*, 8710−8719.

(18) Karpowicz, R. J., Jr., Dunn, M., Sulzer, D., and Sames, D. (2013) APP+, a fluorescent analogue of the neurotoxin MPP+, is a marker of catecholamine neurons in brain tissue, but not a fluorescent false neurotransmitter. *ACS Chem. Neurosci. 4*, 858−869.

(19) Fromherz, P., and Heilemann, A. (1992) Twisted internal charge transfer in (aminophenyl)pyridinium. *J. Phys. Chem. 96*, 6864−6866.

(20) Reichardt, C. (1979) Empirical parameters of solvent polarity as linear free-energy relationships. *Angew. Chem., Int. Ed. 18*, 98.

(21) Koldsø, H., Christiansen, A. B., Sinning, S., and Schiøtt, B. (2013) Comparative modeling of the human monoamine transporters: Similarities in substrate binding. *ACS Chem. Neurosci. 4*, 295−309.

(22) Yamashita, A., Singh, S. K., Kawate, T., Jin, Y., and Gouaux, E. (2005) Crystal structure of a bacterial homologue of Na+/Cl−-dependent neurotransmitter transporters. *Nature 437*, 215−223.

(23) Severinsen, K., Kraft, J. F., Koldsø, H., Vinberg, K. A., Rothman, R. B., Partilla, J. S., Wiborg, O., Blough, B., Schiøtt, B., and Sinning, S. (2012) Binding of the amphetamine-like 1-phenyl-piperazine to monoamine transporters. *ACS Chem. Neurosci. 3*, 693−705.

(24) Shi, L., Quick, M., Zhao, Y., Weinstein, H., and Javitch, J. A. (2008) The mechanism of a neurotransmitter:sodium symporter−

inward release of Na+ and substrate is triggered by substrate in a second binding site. *Mol. Cell 30*, 667−677.
(25) Qian, Y., Galli, A., Ramamoorthy, S., Risso, S., DeFelice, L. J., and Blakely, R. D. (1997) Protein kinase C activation regulates human serotonin transporters in HEK-293 cells via altered cell surface expression. *J. Neurosci. 17*, 45−57.
(26) Wimalasena, D. S., Perera, R. P., Heyen, B. J., Balasooriya, I. S., and Wimalasena, K. (2008) Vesicular monoamine transporter substrate/inhibitor activity of MPTP/MPP+ derivatives: A structure−activity study. *J. Med. Chem. 51*, 760−768.
(27) Vella, S. J., Tiburcio, J., Gauld, J. W., and Loeb, S. J. (2006) Push−pull [2]pseudorotaxanes. Electronic control of threading by switching ON/OFF an intramolecular charge transfer. *Org. Lett. 8*, 3421−3424.
(28) Beuming, T., Shi, L., Javitch, J. A., and Weinstein, H. (2006) A comprehensive structure-based alignment of prokaryotic and eukaryotic neurotransmitter/Na+ symporters (NSS) aids in the use of the LeuT structure to probe NSS structure and function. *Mol. Pharmacol. 70*, 1630−1642.
(29) Leyla, C., Sinning, S., Severinsen, K., Hansen, C. G., Møller, M. S., Bols, M., Wiborg, O., and Schiøtt, B. (2008) Binding of serotonin to the human serotonin transporter. Molecular modeling and experimental validation. *J. Am. Chem. Soc. 130*, 3853−3865.
(30) Koldsø, H., Severinsen, K., Tran, T. T., Celik, L., Jensen, H. H., Wiborg, O., Schiøtt, B., and Sinning, S. (2010) The two enantiomers of citalopram bind to the human serotonin transporter in reversed orientations. *J. Am. Chem. Soc. 132*, 1311−1322.
(31) Suite 2012: Maestro, version 9.3, Schrödinger, LLC, New York, NY, 2012.
(32) Kaminski, G. A., Friesner, R. A., Tirado-Rives, J., and Jorgensen, W. L. (2001) Evaluation and reparametrization of the OPLS-AA force field for proteins via comparison with accurate quantum chemical calculations on peptides. *J. Phys. Chem. B 105*, 6474−6487.
(33) Schrödinger Suite 2012, MacroModel, version 9.6, Schrödinger, LLC, New York, NY, 2012.
(34) Sherman, W., Day, T., Jacobson, M. P., Friesner, R. A., and Farid, R. (2006) Novel procedure for modeling ligand/receptor induced fit effects. *J. Med. Chem. 49*, 534−553.
(35) Schrödinger Suite 2012, Glide, version 5.8, Schrödinger, LLC, New York, NY, 2012.
(36) Schrödinger Suite 2012, Prime, version 3.1, Schrödinger, LLC, New York, NY, 2012.
(37) Friesner, R. A., Banks, J. L., Murphy, R. B., Halgren, T. A., Klicic, J. J., Mainz, D. T., Repasky, M. P., Knoll, E. H., Shelley, M., Perry, J. K., Shaw, D. E., Francis, P., and Shenkin, P. S. (2004) Glide: A new approach for rapid, accurate docking and scoring. 1. Method and assessment of docking accuracy. *J. Med. Chem. 47*, 1739−1749.
(38) Sinning, S., Musgaard, M., Jensen, M., Severinsen, K., Celik, L., Koldsø, H., Meyer, T., Bols, M., Jensen, H. H., Schiøtt, B., and Wiborg, O. (2010) Binding and orientation of tricyclic antidepressants within the central substrate site of the human serotonin transporter. *J. Biol. Chem. 285*, 8363−8374.
(39) Friesner, R. A., Murphy, R. B., Repasky, M. P., Frye, L. L., Greenwood, J. R., Halgren, T. A., Sanschagrin, P. C., and Mainz, D. T. (2006) Extra precision glide: Docking and scoring incorporating a model of hydrophobic enclosure for protein-ligand complexes. *J. Med. Chem. 49*, 6177−6196.
(40) Cho, A. E., Guallar, V., Berne, B. J., and Friesner, R. (2005) Importance of accurate charges in molecular docking: quantum mechanical/molecular mechanical (QM/MM) approach. *J. Comput. Chem. 26*, 915−931.
(41) Schrödinger Suite 2012, Jaguar, version 7.9, Schrödinger, LLC, New York, NY, 2012.
(42) Schrödinger Suite 2012, Canvas, version 1.5, Schrödinger, LLC, New York, NY, 2012.